

Mechanistic Investigation of Chiral Phosphoric Acid Catalyzed Asymmetric Baeyer–Villiger Reaction of 3-Substituted Cyclobutanones with H₂O₂ as the Oxidant

Senmiao Xu,^[a] Zheng Wang,^[a] Yuxue Li,^{*,[a]} Xumu Zhang,^[b] Haiming Wang,^[a] and Kuiling Ding^{*,[a]}

Abstract: The mechanism of the chiral phosphoric acid catalyzed Baeyer–Villiger (B–V) reaction of cyclobutanones with hydrogen peroxide was investigated by using a combination of experimental and theoretical methods. Of the two pathways that have been proposed for the present reaction, the pathway involving a peroxyphosphate intermediate is not viable. The reaction progress kinetic analysis indicates that the reaction is partially inhibited by the γ -lactone product. Initial rate measurements suggest that the reaction follows Michaelis–Menten-type kinetics consistent with a bifunctional mechanism in which the catalyst is actively involved in both carbonyl addition and the subsequent rearrangement steps

through hydrogen-bonding interactions with the reactants or the intermediate. High-level quantum chemical calculations strongly support a two-step concerted mechanism in which the phosphoric acid activates the reactants or the intermediate in a synergistic manner through partial proton transfer. The catalyst simultaneously acts as a general acid, by increasing the electrophilicity of the carbonyl carbon, increases the nucleophilicity of hydrogen peroxide as a Lewis base in the addition

step, and facilitates the dissociation of the OH group from the Criegee intermediate in the rearrangement step. The overall reaction is highly exothermic, and the rearrangement of the Criegee intermediate is the rate-determining step. The observed reactivity of this catalytic B–V reaction also results, in part, from the ring strain in cyclobutanones. The sense of chiral induction is rationalized by the analysis of the relative energies of the competing diastereomeric transition states, in which the steric repulsion between the 3-substituent of the cyclobutanone and the 3- and 3'-substituents of the catalyst, as well as the entropy and solvent effects, are found to be critically important.

Keywords: asymmetric catalysis • Baeyer–Villiger reaction • density functional calculations • kinetics • organocatalysis

Introduction

The Baeyer–Villiger (B–V) oxidation, which converts ketones into the corresponding esters or lactones, is of great importance in organic synthesis due to its predictable regio- and stereoselectivity.^[1] Since its discovery by Baeyer and Villiger in 1899,^[2] considerable progress has been made to understand the mechanism of the reaction and to use this reaction in preparative chemistry.^[3–6] In the vast majority of cases, B–V reactions have been performed with an organic peracid, such as *m*-chloroperbenzoic acid (*m*CPBA), as the oxidant. However, in some cases, hydrogen peroxide has been successfully employed in combination with a catalyst; this offers a number of advantages in terms of environmental and economical concerns. For the B–V oxidation with a peroxycarboxylic acid in the absence of acid/base catalysis, it is generally accepted that the reaction proceeds through a

[a] Dr. S. Xu, Prof. Dr. Z. Wang, Prof. Dr. Y. Li, H. Wang, Prof. Dr. K. Ding
State Key Laboratory of Organometallic Chemistry
Shanghai Institute of Organic Chemistry
Chinese Academy of Sciences, 354 Fenglin Road
Shanghai 200032 (P.R. China)
Fax: (+86) 21-6416-6128
E-mail: kding@mail.sioc.ac.cn
liyuxue@mail.sioc.ac.cn

[b] Prof. Dr. X. Zhang
Department of Chemistry and Chemical Biology
Center of Molecular Catalysis, Rutgers
The State University of New Jersey, 610 Taylor
Piscataway, New Jersey 08854 (USA)

Supporting information for this article is available on the WWW under <http://dx.doi.org/10.1002/chem.200902698>.

two-step mechanism. Initially, the peracid attacks the carbonyl carbon of the ketone or aldehyde, leading to the formation of a tetrahedral perhemiketal species, known as the Criegee intermediate.^[7] Then, the intermediate undergoes an intramolecular migration of an alkyl or aryl substituent from the central carbon to the proximal oxygen of the perester moiety, resulting in the production of the ester (or lactone) and a carboxylic acid. The B–V oxidation with hydrogen peroxide is also often hypothesized to proceed in a similar manner, but the reaction needs some kind of catalyst for sufficient reactivity and selectivity, and various catalysts have been used, including homogeneous Brønsted acids,^[8–12] heterogeneous solid acids,^[13] flavin-based organocatalysts,^[14,15] Lewis acidic transition-metal complexes,^[5] and Lewis acidic metal incorporated into molecular sieves.^[6] Despite such a general understanding, however, in many cases the detailed mechanism of the reaction has been found to be unclear and some key issues are still debated. For example, the migration has often been proposed to be the rate-determining step, which involves a concerted formation of a C–O bond with the simultaneous cleavage of the O–O bond. However, some studies have shown that the carbonyl addition can also be rate determining and can depend on the reaction conditions as well as the reactants.^[3,16–18] For the carbonyl addition step, there is still no consensus on whether the protonation of the carbonyl oxygen and the carbonyl addition occur in a stepwise or concerted manner.^[19] Besides, there are some controversies with regards to the potential effect of the acid, which is generated as a byproduct during the reaction and may catalyze both steps.^[18] Overall, the B–V reaction cannot be explained by a single mechanism and the detailed mechanism of the reaction varies with the catalyst, substituent effect, solvent, and/or acidity.^[3]

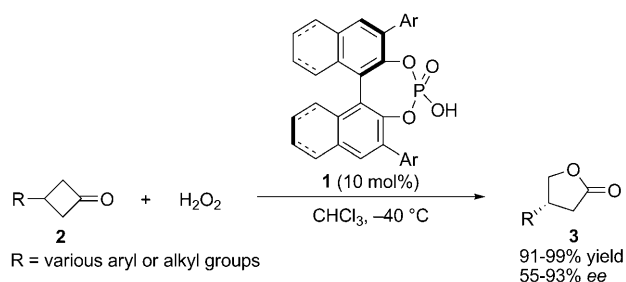
The mechanism of the B–V reaction has also been the subject of a number of theoretical studies. Most of these studies have investigated B–V reactions with peroxy-carboxylic acids as oxidants.^[17–23] Remarkably, even though calculations indicated that the reactions can be catalyzed by general acid catalysis, through hydrogen-bond formation, there are still some contradictory results in the mechanism elucidation with regards to the molecularity and the mode of activation.^[21,23] For the mechanism elucidation of the B–V oxidation with hydrogen peroxide, only a few computational studies have been published.^[24–27] Carlqvist and co-workers studied the uncatalyzed and BF₃-assisted B–V oxidation of acetone with hydrogen peroxide using high-level *ab initio* and DFT methods and found that both steps in the uncatalyzed reaction have very high activation barriers, which is in agreement with the experimental observation that B–V reactions of ketones with hydrogen peroxide does not occur to a significant extent without catalytic activation.^[24] It was found that the Lewis acidic BF₃ facilitates both steps of the reaction and significantly lowers the activation barrier for the rate-determining step (from 49.0 to 17.0 kcal mol⁻¹). Sever and Root investigated several possible mechanisms for Sn- and Ti-catalyzed B–V oxidations of acetone with hydrogen peroxide using a DFT method.^[25] The calculations

indicated that the catalyzed reactions proceed through a Criegee intermediate that contains a five-membered chelate ring involving the tin center, which effectively activates both reactants in the addition step and facilitates the departure of hydroxyl group in the following rearrangement. Corma and co-workers have studied the B–V oxidation of cyclohexanone with hydrogen peroxide catalyzed by the Sn beta-zeolite using a combination of molecular mechanics, quantum chemical calculations, and spectroscopic and kinetic techniques.^[26] The zeolite active site was found to consist of two catalytic centers: the Lewis acidic Sn atom for activation of cyclohexanone by coordination, and an adjacent basic oxygen atom of the Sn–OH group for interaction with H₂O₂ by hydrogen-bond formation. It should be noted that from these studies valuable insights can be obtained on the molecular pathways of the reactions, however, the lack of experimental data on many calculated systems might also hinder further mechanistic understanding and corroboration.

On the other hand, catalytic asymmetric B–V oxidation of cyclic ketones provides a rapid access to various chiral lactones, which are valuable synthetic intermediates and have found widespread biochemical applications. Thus, it is not surprising to see that a continuous effort has been made to search for more efficient chiral catalysts, either natural or synthetic, to accomplish this reaction in an enantioselective manner.^[28] In this arena, enzymatic systems are highly enantioselective, but, by their nature, exhibit substrate specificity.^[29,30] Chemical catalysts offer an attractive alternative, especially reactions using environmentally benign oxidants such as H₂O₂, but they are still limited in number and are often less enantioselective than their biological counterparts.^[5] Since the first reports on metal-catalyzed asymmetric B–V reactions in 1994,^[31] various chiral metal catalysts based on Cu^{II},^[32] Pt^{II},^[33] Ti^{IV},^[34] Co^{III},^[35] Zr^{IV},^[36] Mg^{II},^[37] Al^{III},^[38] and Pd^{II}^[39] have been developed in recent years for this transformation. However, so far, very few of them could attain enantioselectivity at a level comparable to enzymes, and wide substrate generality has not yet been achieved in each case. Complementary to metal catalysis, several chiral organocatalysts based on organoseleniums,^[40] flavins,^[15] amino acids,^[41] and organophosphoric acids^[42] have also been demonstrated to be a useful and green alternative for the conversion. With regards to mechanistic aspects of the catalytic B–V reactions, Strukul and co-workers have investigated some Pt^{II} and Pd^{II} complexes of achiral diphosphines using a combination of kinetic and spectroscopic techniques.^[43,44] However, to the best of our knowledge, the chiral Brønsted acid catalysis of B–V reactions has never been studied in great detail, and there is no computational study that has considered catalytic enantioselective B–V reactions.

We have previously reported that chiral organophosphoric acids based on enantiopure 1,1'-bi-2-naphthol (BINOL)^[42] derivatives are competent catalysts for the enantioselective B–V oxidation of 3-substituted cyclobutanones with aqueous H₂O₂ (30%) as the oxidant, affording the corresponding γ -

lactones in excellent yields with enantiomeric excess (*ee*) values up to 93% (Scheme 1).^[42] However, further attempts to expand the strategy to other less-strained cyclic ketones



Scheme 1. BINOL-derived chiral phosphoric acid catalyzed enantioselective B–V reaction of cyclobutanone derivatives.

(cyclopentanone, cyclohexanone, or diphenylketone) were unsuccessful, with no conversion being detected at ambient temperature. To rationalize the origin of the reactivity differences among the ketone substrates and to understand some key issues of the reaction (including the plausible mechanistic pathway(s) and the kinetics, the effects of the chiral phosphoric acid, as well as the controlling factors with respect to the enantioselectivity), we undertook a combined experimental and theoretical study of the B–V oxidation of cyclobutanones with aqueous H_2O_2 catalyzed by chiral phosphoric acids. Insights into the mechanism are gained by the nonlinear effect (NLE), NMR spectroscopic analysis, and kinetic analysis of the system, whereas further details regarding the geometries and energy profiles of the transition structures and intermediates are provided by a theoretical study using quantum chemical calculations. The results obtained in this study underline the acid/base bifunctional nature of the organophosphoric acid catalyst, which plays a key role in facilitating both steps in the catalytic cycle through hydrogen-bond formation with the reactants and the intermediate.

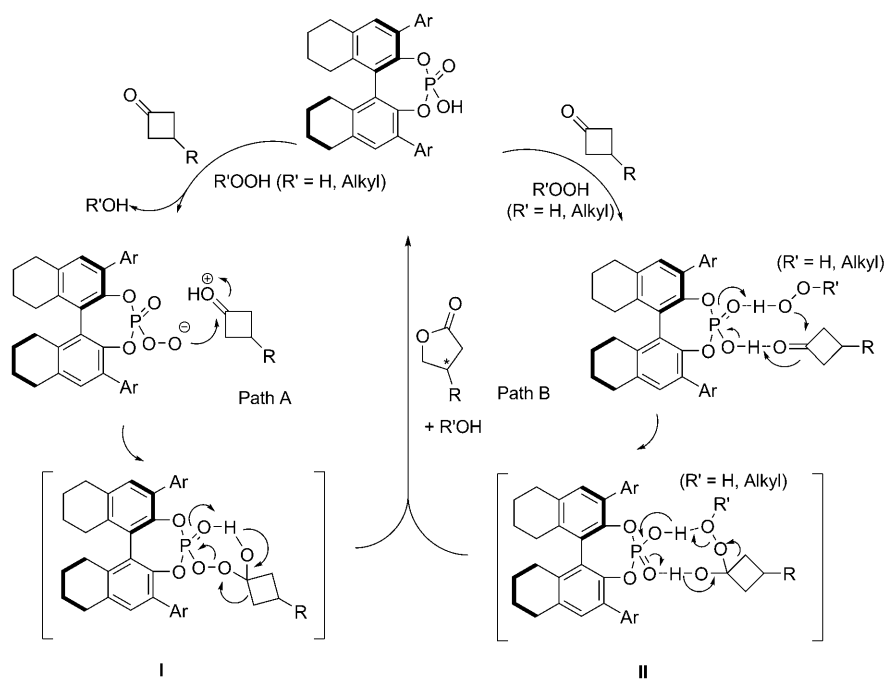
Results and Discussion

The peroxyphosphoric acid pathway and the general acid pathway: The NLE has been recognized as an important phenomenon that contains rich mechanistic information in enantioselective catalysis, and has often been used as a powerful diagnostic tool to probe the nature, and especially the aggregation behavior, of the catalytic species involved.^[45] With regards to the nature of the catalytic species involved in the title reaction, we have previously reported an NLE investigation of this system.^[42] The study has shown that the *ee* values of the product are proportional to those of the catalyst, clearly indicating the absence of an NLE in this reaction. Moreover, changes in catalyst concentration at room temperature do not result in substantial impact on the enantioselectivity of the catalysis.^[42] These phenomena strongly

indicate that only a single molecule of the phosphoric acid is involved in the catalytic cycle.

Then what is the exact identity of the catalytic species? On the basis of the commonly accepted B–V mechanism for peroxydicarboxylic acids, we have proposed the involvement of a peroxyphosphate intermediate, whereas List and Müller suggested an alternative bifunctional mechanism involving noncovalent interactions between the phosphoric acid and the reactants or the Criegee intermediate.^[46] Peroxyphosphoric acid would presumably be generated in situ by the reaction of phosphoric acid with hydrogen peroxide, and a route involving this intermediate would have the advantage of being similar to the well-known mechanism of the stoichiometric B–V oxidation using various peracids. For example, Ogata and co-workers have performed an elegant study on the kinetics of the B–V reaction of acetophenones with permonophosphoric acid, which was prepared in situ by the reaction of P_2O_5 with H_2O_2 in MeCN.^[47] Analogously, per-seleninic acids have also often been invoked as the true active species for a number of B–V oxidations using hydrogen peroxide with various organoselenium catalysts.^[9,10,12] On the other hand, the bifunctional nature of the phosphoric acid in some asymmetric catalytic reactions has been well documented in the literature.^[48–50] It was found that phosphoric acid has a proton of considerable acidity, whereas the presence of the Lewis basic phosphoryl moiety, in proximity to the acidic proton, may potentially allow for bifunctional catalysis, that is, simultaneous activation of both electro- and nucleophilic reaction partners.^[51] Therefore, two possible pathways for the B–V reaction, in which a single molecule of phosphoric acid can be involved in the catalytic cycle either as a peroxyphosphoric acid (path A) or as a bifunctional general acid (path B) were considered for the present mechanistic study (Scheme 2).

An inspection of paths A and B in Scheme 2 reveals two important features that may be potentially useful in the differentiation of the routes. First, new signals in the ^{31}P NMR spectrum would be expected upon formation of the peroxy species in path A, whereas in path B, the chemical shift of the ^{31}P NMR signal of the catalyst may not change significantly considering the relatively weak noncovalent interactions. Second, the enantioselectivity of the reaction proceeding by path A should be independent of the oxidant used ($\text{R}'\text{OOH}$, $\text{R}' = \text{H}$ or alkyl), since a common Criegee intermediate **I** is involved in the reaction, whereas the reverse should be true for path B, in which the alkyl substituent group in $\text{R}'\text{OOH}$ persists near the reactive sites in both steps of the catalysis. It should be noted that when using alkylhydroperoxides as the oxidants, both the formation of the peroxyphosphoric acid in path A (Scheme 2) and the corresponding peroxyester (not shown in path A of Scheme 2) are possible by release of alcohols or H_2O , respectively. However, the peroxyester is expected to be inactive for B–V reactions because it lacks an acidic proton. In fact, comparison of the ^{31}P NMR spectra of the phosphoric acid **1a** taken in CDCl_3 before and after the addition of 15 equivalents of a 30% aqueous solution of H_2O_2 reveals a



Scheme 2. Two plausible pathways for the chiral phosphoric acid catalyzed B–V oxidation of 3-substituted cyclobutanones by using R'OOH (R' = H or alkyl) as oxidants.

slight upfield change in chemical shift ($\delta = 4.29$ to 4.60 ppm) after standing for 24 h at RT, suggesting that the hypothetical formation of the peroxyphosphate species in path A is unlikely under the reaction conditions (Figure 1).^[52] Furthermore, different oxidants were employed to assess the enantioselectivity for the catalytic B–V reaction of 3-phenyl cyclobutanone **2a** with **1b** as the catalyst under otherwise identical conditions. The results have shown that the *ee* values of the lactone **3a** vary significantly with the oxidant employed (Table 1), which is consistent with path B (Scheme 2). In addition, three computational models were studied to estimate the activation barrier for the oxidation of the 5,5',6,6',7,7',8,8'-octahydro-1,1'-bi-2-naphthol (H_8 -BINOL)-derived phosphoric acid (**1c**) to the corresponding peroxy species with or without the assistance of water

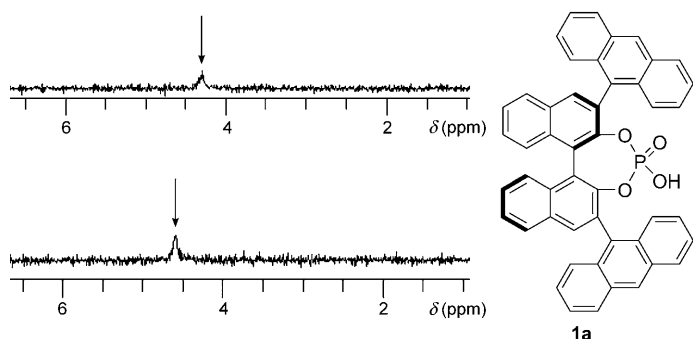


Figure 1. Comparison of ^{31}P NMR spectra of the phosphoric acid **1a** in the presence (top; $\delta = 4.292$ ppm) or absence of H_2O_2 (bottom; $\delta = 4.579$ ppm).

(Figure 2). The calculated Gibbs activation barriers are all higher than 33 kcal mol^{-1} (calculated at the B3LYP/6-311+G** level with solvent effect taken into account), which means that no peroxyphosphoric acid would form under the reaction conditions (ambient or lower temperatures). On the basis of these experimental findings and the calculation results, the possibility of the reaction proceeding by way of a peroxyphosphoric acid species (path A) can be safely excluded from further considerations.

Kinetic studies: To gain further insights into the mechanism of the B–V reaction, an extensive kinetic study was carried out. Kinetic data were obtained from the B–V oxidation of 3-*n*-

Table 1. Asymmetric B–V reaction of **2a** by using different oxidants in the presence of catalyst **1b**.^[a]

| Entry | Oxidant | Time [h] | Yield ^[b] [%] | <i>ee</i> ^[c] [%] |
|-------|-----------------------------|----------|--------------------------|------------------------------|
| 1 | 30 % H_2O_2 | 12 | 99 | 71 |
| 2 | TBHP | 36 | 87 | 17 |
| 3 | CHP | 36 | 92 | 15 |

[a] All reactions were carried out at room temperature with $[\mathbf{2a}] = 0.1 \text{ M}$ and 1.5 equiv of oxidant. [b] The yield of isolated product. [c] The enantiomeric excess of **3a** was determined by chiral HPLC. TBHP = *tert*-butyl hydroperoxide, CHP = cumene hydroperoxide.

hexylcyclobutanone (**2b**) by 30% aqueous H_2O_2 using catalyst **1b**, and the reaction was performed at 27°C in dichloromethane (Scheme 3). The consumption of **2b** was monitored by gas chromatography with *n*-dodecane as an internal standard.

Because the reaction medium is biphasic (dichloromethane/water), possible influences of mass transfer limitations of the reagents back and forth between the phases has to be taken into account, and it is necessary to take precautions to ensure that the reaction rate is not diffusion controlled. Indeed, reaction profiles obtained under different stirring

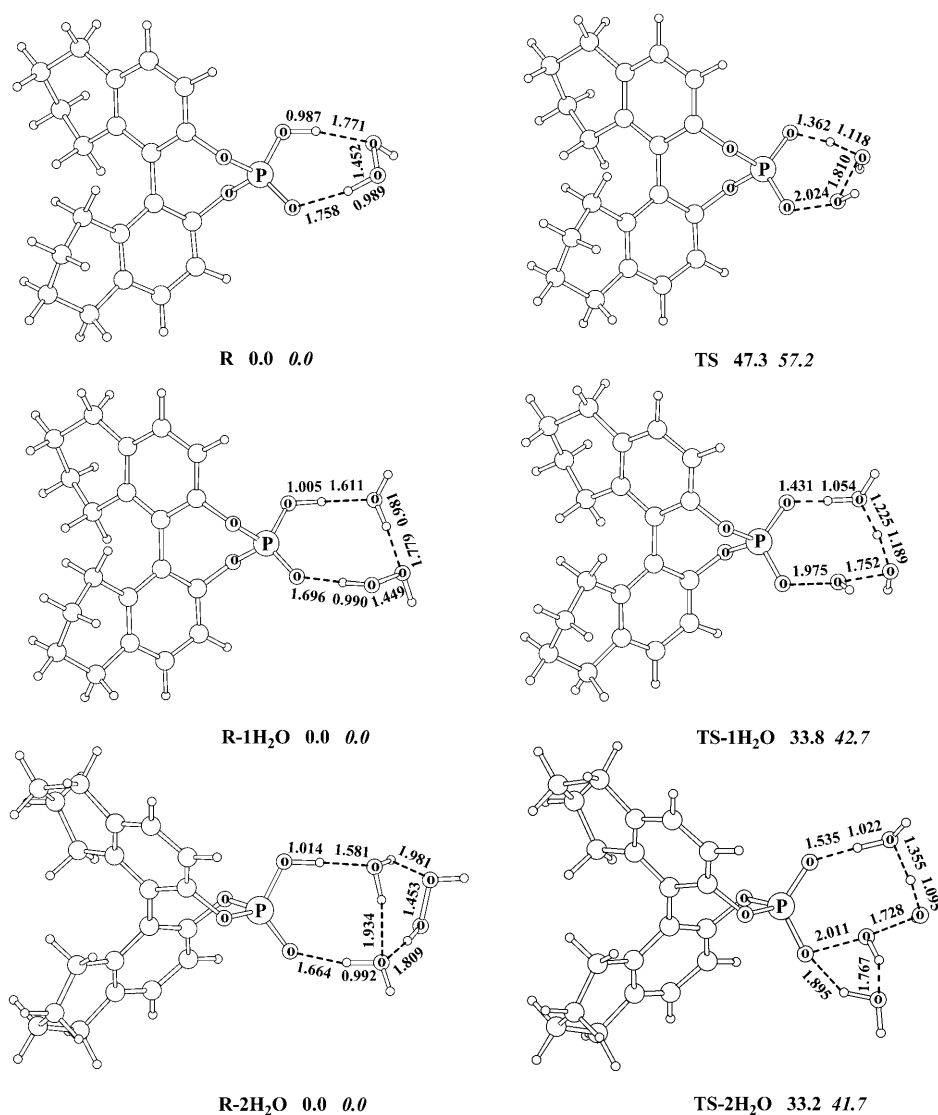
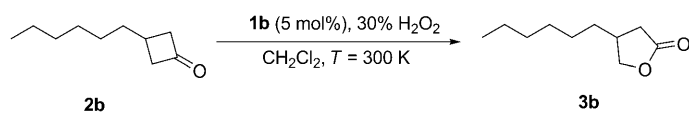


Figure 2. The optimized structures with selected bond lengths (in Å) of the reaction complex **R** and the corresponding transition states (TS) for the oxidation of the phosphoric acid **1c** by hydrogen peroxide, with or without the assistance of water. The geometries were fully optimized at the B3LYP/6-311+G** level. The relative energies $\Delta G_{\text{B3LYP-Sol}}$ (in bold) and $\Delta G_{\text{MP2-Sol}}$ (in italic) are in kcal mol⁻¹ (for the details of the calculation, see the Theoretical Calculations section).



Scheme 3. The model B–V reaction for kinetic studies.

rates (Figure S2 in the Supporting Information) clearly indicate some influences of mass transfer on the reaction under a stirring rate lower than 900 rpm, since the plots deviate significantly from each other in these cases. Nevertheless, the plots are essentially reproducible at a stirring rate of about 1000 rpm, indicating that mass transfer under such circumstances would no longer be rate determining. Therefore,

the stirring rates were fixed to 1000 rpm in subsequent kinetic experiments.

To obtain a comprehensive picture of the kinetic behavior for the B–V oxidation, a reaction progress kinetic analysis was performed by following the elegant strategy developed by Blackmond.^[53] By monitoring the entire course of the reaction under synthetically relevant conditions, such a method allows for a rapid kinetic analysis of a complex catalytic reaction with a minimal number of experiments, and can provide significant information about complicating issues such as catalyst incubation, catalyst deactivation, or product inhibition. According to the principles described by Blackmond,^[53] hydrogen peroxide was the reactant used in excess, a quantity defined as the difference in total molar concentration between the two substrates for the present case. Although the whole amount of hydrogen peroxide is partitioned between the aqueous and organic phases,^[44,54] the total molar concentration of H₂O₂ in the whole system is used here instead of its actual concentration in the organic phase. This does not affect the meaning of the results, as is clear from a similar kinetic study by Strukul and co-workers on the Pt^{II}-catalyzed alkene epoxidation with H₂O₂ in chlorinated solvents.^[55] For

the present reaction, the rate is now plotted against the concentration of cyclobutanone **2b** in Figure 3, line a, and indicates that the reaction is approximately first order in cyclobutanone. However, when the reaction was carried out with an increased initial cyclobutanone and hydrogen peroxide concentration, but at the same excessive [H₂O₂], the new plot does not overlay to the original one and shows a somewhat lowered rate (line b in Figure 3). This behavior indicates that the total concentration of active catalysts varies with the reaction progress, as a result of either catalyst deactivation or product inhibition. This was further investigated by adding a certain amount of lactone product **3b** to the reaction system, while keeping the other conditions identical to those of the first experiment. Indeed, the approximate

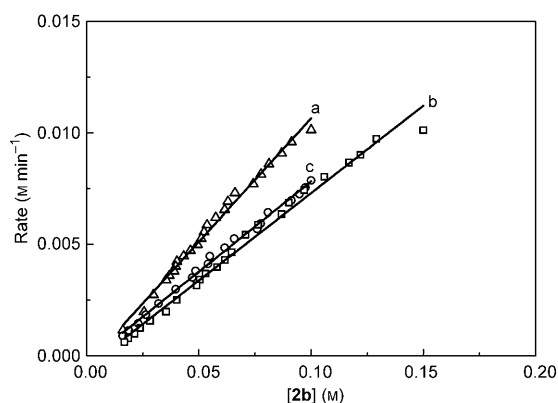


Figure 3. Plots of reaction rates against various initial cyclobutanone concentrations, standard conditions: **[1b]** = 5 mM in 2 mL of CH₂Cl₂, *T* = 300 K, stirring rate = 1000 rpm. Δ : **[2b]** = 0.10 M, [H₂O₂] = 0.15 M, [H₂O₂]_{excess} = 0.05 M; \square : **[2b]** = 0.15 M, [H₂O₂] = 0.20 M, [H₂O₂]_{excess} = 0.05 M; \circ : **[2b]** = 0.10 M, [H₂O₂] = 0.15 M, [H₂O₂]_{excess} = 0.05 M, **[3b]** = 0.05 M.

overlap of the new data curve (line c in Figure 3) with that shown in Figure 3, line b attests that product inhibition is responsible in this case (see also Figure S3 in the Supporting Information). This is reasonable considering that the lactone carbonyl group can compete with cyclobutanone for hydrogen-bonding interactions with the catalyst. However, in such a case, the effective concentration of the active catalyst would change considerably with the reaction progress, which would complicate the kinetic analysis.

On the basis of the reaction process data mentioned above, the initial rate analysis was used to further assess the kinetic aspects of the present reaction to minimize the influence of product inhibition. As can be seen from Figures S5–S7 in the Supporting Information, the initial rate remains nearly constant for a typical reaction profile within 3 min when the conversion was less than 20%, and can be determined with reasonable accuracy. Points at the end of the run when the catalyst had presumably been trapped in part by the product were discarded. Accordingly, kinetic data were obtained by varying in turn the initial concentrations of H₂O₂, the substrate, and the catalyst. To this end, rate studies were conducted on a series of B–V reactions in CH₂Cl₂ at 300 K, and aliquots were withdrawn periodically from the reaction mixture for GC analysis. The dependence of initial rate on the concentration of hydrogen peroxide was first examined with the B–V reaction of **2b** (0.1 M in CH₂Cl₂) and concentrations of H₂O₂ ranging from 0.10 to 0.30 M in the presence of 5 mol% catalyst. Interestingly, the rates of the cyclobutanone conversion were found to be approximately independent of H₂O₂ concentration under the conditions tested (Figure 4). As far as the mechanism is concerned, the independence of substrate conversion and the H₂O₂ concentration implied that the step involving H₂O₂, either the association with the catalyst or the nucleophilic attack on the carbonyl carbon, should be a relatively facile one in the catalytic cycle.

Subsequently, the rate dependence with respect to the initial concentration of catalyst **1b** (1.25–5 mM) was evaluated

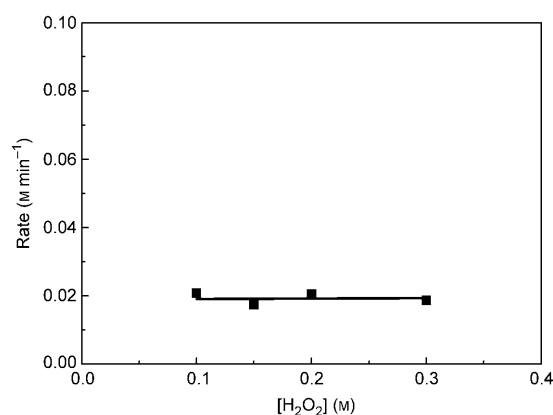


Figure 4. Plot of initial rate against [H₂O₂] in the presence of **1b** (5 mM) at 27 °C (300 K) (**[2b]** = 0.1 M in CH₂Cl₂).

by using the B–V reaction of cyclobutanone **2b** (0.1 M in CH₂Cl₂) with H₂O₂ (0.15 M) at 27 °C. As shown in Figure 5, an approximately linear correlation between the reaction

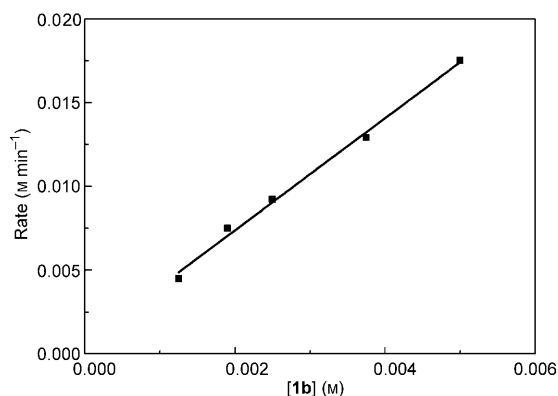


Figure 5. Plot of initial rate of **2b** (0.1 M in CH₂Cl₂) with H₂O₂ (0.15 M) against **[1b]** (1.25 to 5 mM) at 27 °C (300 K). $y = 3.34428x + 0.00069$, $R^2 = 0.9936$.

rate and the concentration of **1b** was obtained, reflecting a nearly first-order dependence on catalyst. This is consistent with the aforementioned results from NLE studies, which suggested that only a single catalyst molecule is involved in the rate-determining step. The small intercept on the y axis indicates that the contribution from a noncatalyzed oxidation of cyclobutanone is negligible, again confirming that the reaction does not occur without a catalyst.^[42]

Finally, the influence of the concentration of **2b** (0.04–0.12 M in CH₂Cl₂) on the reaction rate was examined in the presence of **1b** (2.5 mM) and H₂O₂ (0.15 M) at 300 K to ascertain the kinetic order with respect to the ketone substrate. The profiles indicate no incubation period in the reaction (Figure S7 in the Supporting Information), which suggests that catalyst preactivation is not required for the reaction to occur. Figure 6 depicts the plot of initial rate against the concentration of **2b** (conversion < 20%), which indicates

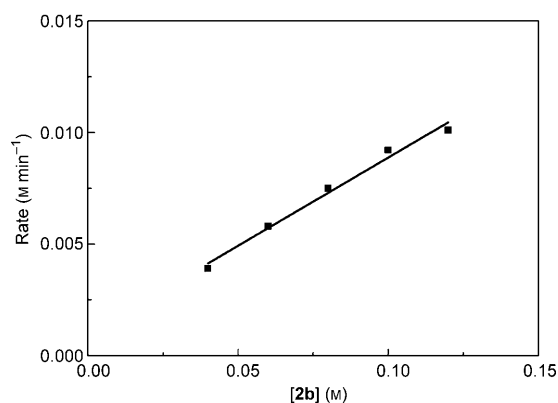


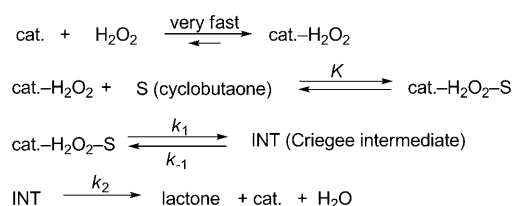
Figure 6. Plot of initial reaction rate against **[2b]** (from 0.04 to 0.12 M in CH₂Cl₂) in the presence of H₂O₂ (0.15 M) and **1b** (2.5 mM) at 27°C (300 K). $y = 0.079x + 0.00098$; $R^2 = 0.9823$.

that the rate for the process is approximately first order in the ketone substrate.

Therefore, the B–V reaction of **2b** with H₂O₂ catalyzed by **1b** at 27°C (300 K) in CH₂Cl₂ proceeds by approximately following the initial rate law shown in Equation (1). It should be emphasized that this is an empirical approximate initial rate equation. In this case, the γ -lactone concentration is zero at the beginning of the reaction, and its concentration effect is not obvious in the kinetic equation.

$$\text{Rate} \approx k[\mathbf{1b}]^1[\mathbf{2b}]^1[\text{H}_2\text{O}_2]^0 \quad (1)$$

On the basis of these kinetic results, we propose a refined catalytic cycle as outlined in Scheme 4. Addition of more H₂O₂ does not lead to a rate enhancement, which is consistent with a rapid saturation of the catalytic sites with H₂O₂ through hydrogen-bonding association at the beginning of the reaction. This pre-equilibrium should be a fast and kinetically indistinguishable process. It is worth noting that chiral organophosphoric acids are known to be amphiphilic,^[56] with a hydrophilic acidic interior being sandwiched between the hydrophobic binaphthalene skeleton and the 3- and 3'-substituent groups. Although the effective concentration of H₂O₂ in dichloromethane is expected to be very small compared with that of cyclobutanone due to mutual immiscibility,^[44,54] a hydrogen-bonding complex $\text{cat.}-\text{H}_2\text{O}_2$ is preferentially formed probably at the interface between the aqueous and organic phases. Further interaction of this complex with the cyclobutanone substrate S would lead to the



Scheme 4. A refined catalytic cycle based on kinetic studies.

reversible formation of a hydrogen-bonded termolecular array $\text{cat.}-\text{H}_2\text{O}_2-\text{S}$. An intra-supramolecular nucleophilic attack of H₂O₂ on the cyclobutanone within the array results in the formation of the catalyst-bonded Criegee intermediate, which undergoes a subsequent migration–rearrangement to afford the lactone with the release of the catalyst. However, the simple kinetic analysis here does not distinguish whether the addition to the carbonyl to form the Criegee intermediate (INT) or its subsequent rearrangement to the lactone is the rate-determining step, because the rate equation would be the same in both cases. This issue will be further clarified by quantum chemical calculations (see below).

This overall reaction sequence is reminiscent of the Michaelis–Menten two-step enzyme kinetics typical of those encountered in enzyme-catalyzed biochemical reactions. Indeed, a better correlation was obtained in the present catalytic system by plotting the experimental data according to the double-reciprocal equation developed by Lineweaver and Burk.^[57] For the sequence outlined in Scheme 4, postulating the steady-state concentration of the Criegee intermediate (INT) and using material conservations can lead to the double-reciprocal expression given in Equation (2) after simple algebraic manipulations.

$$\frac{1}{\text{Rate}} = \frac{k_1 + k_{-1} + k_2}{k_1 k_2 [\text{cat.}]_0} + \frac{k_{-1} + k_2}{k_1 k_2 K [\text{cat.}]_0 [\text{S}]} = b + \frac{a}{[\text{S}]} \quad (2)$$

The constants k_1 , k_{-1} , k_2 , and K are rate or equilibrium constants of the elementary steps defined in Scheme 4, and $[\text{cat.}]_0$ and $[\text{S}]$ are the initial concentrations of the catalyst and cyclobutanone substrate, respectively. Based on the data from the initial rate measurement, an excellent linear relationship (with an R^2 value of 0.997) is obtained by fitting the experimental data into the double-reciprocal equation [Eq. (2); Figure 7]. Therefore, the initial rate of the reaction is strictly first order in the catalyst, but shows a more complex dependence on the concentration of the cyclobutanone substrate. This can be seen from an equation of rate dependence on substrate concentration [Eq. (3)], which is further

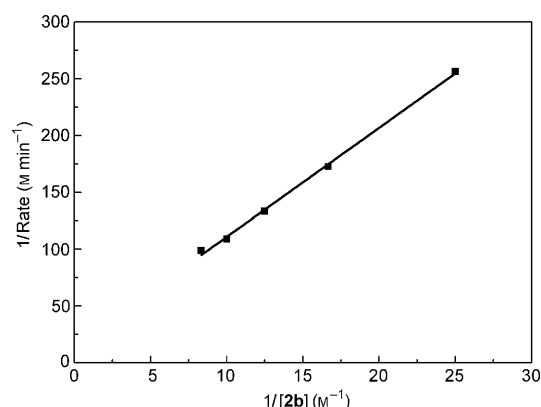


Figure 7. The Lineweaver–Burk plot of the B–V reaction of **2b** in the presence of H₂O₂ (0.15 M) and **1b** (2.5 mM) in CH₂Cl₂ at 300 K. $y = 9.59x + 14.92$; $R^2 = 0.9973$.

deduced from Equation (2), in which a and b are 9.59 and 14.92, respectively, for the present catalytic system (see Figure 7).

$$\text{Rate} = \frac{[S]}{b[S] + a} \quad (3)$$

At a low concentration of the ketone substrate (e.g., $[2b] = 0.030\text{--}0.125\text{ M}$ as shown in Figure 6), the term $b[S]$ ranges from 0.45 to 1.94, which is much smaller than the a value (9.59). Thus, the denominator $b[S] + a \approx a$, so that under low concentrations of $2b$ the rate $\approx [S]/a$. This implies that the rate is approximately proportional to the concentration of cyclobutanone in a relatively dilute solution, such as the cases shown in Figure 6. Accordingly, the intercept b on the y axis of the Lineweaver–Burk plot is an indication of kinetic behavior sensitivity of the ketone with the change of its concentration. Equation (1) can be regarded as an approximation of Equation (2) when the cyclobutanone concentration is low enough, and Equation (2) is more rigorous mathematically and more accurately reflects the kinetic behavior of the catalytic system.

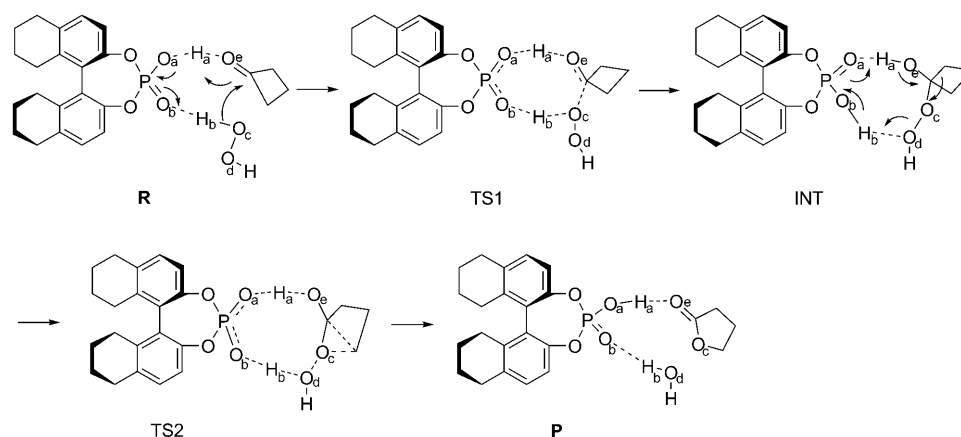
Theoretical calculations: To gain further insights into the mechanism, a theoretical study was carried out to explore the geometries and energetics of the key species as well as to rationalize the reactivity/enantioselectivity of the catalysis. A plausible mechanistic pathway is shown in Scheme 5, in which the H_8 -BINOL-derived phosphoric acid acts as a bifunctional catalyst throughout the catalytic sequence to form hydrogen-bonding networks with the reactants, Criegee intermediate, or the lactone product. The BINOL-derived phosphoric acids contain both a Brønsted acidic site (acid proton) and a Lewis basic site (phosphoryl oxygen) in proximity, and have been proposed to activate simultaneously both electrophilic and nucleophilic reaction partners by hydrogen-bond formation in a number of reactions.^[49–51,58] Such a bifunctional catalysis pattern has also been demonstrated to be viable in several recent theoretical studies on the mechanisms of phosphoric acid catalyzed nucleophilic addition reactions of imines, including Hantzsch ester trans-

fer hydrogenations,^[59,60] Strecker reactions,^[61] and hydrophosphonylation.^[62–63]

Computational details: All calculations in this work were performed with density functional theory (DFT)^[64] and MP2^[65] implemented in the Gaussian 03 program.^[66] For the exploration of the reaction pathway shown in Scheme 5 and the following reactivity calculations, (*R*)- H_8 -BINOL-derived phosphoric acid (**1c**) was used as the model catalyst, in which the initial conformation of the binaphthyl rings was kept the same as that in the H_8 -BINOL/Ti complex, which has been characterized by X-ray crystallography.^[67] Models were constructed and fully optimized at the B3LYP^[68]/6-311+G** level. For each optimized structure, a harmonic vibrational frequency calculation was carried out and thermal corrections were made. All structures were shown to be either transition states (with one imaginary frequency) or local minima (with no imaginary frequency). The solvent effect was estimated with IEFPCM^[69] (UAHF atomic radii) method in chloroform ($\epsilon = 4.9$) using the gas-phase optimized structures. The MP2/6-311+G** single-point calculation was performed to obtain more accurate energies.

The optimized structures for the species proposed in Scheme 5 are depicted in Figure 8, along with the calculated Gibbs free energy profiles for the corresponding mechanistic pathway. Two types of relative free energies (in kcal mol⁻¹), both with the hydrogen-bonded termolecular complex **R** as the zero reference point, are shown in Figure 8. The $\Delta G_{\text{B3LYP-Sol}}$ values correspond to the relative free energies calculated with the B3LYP/6-311+G** method plus the solvent effect, whereas $\Delta G_{\text{MP2-Sol}}$ are MP2/6-311+G** single-point energies plus the thermal free energy corrections and the solvent effect at the B3LYP/6-311+G** level.

The reactant complex (R): For the initial step of the catalytic B–V reaction, the calculation starts with a termolecular reactant complex **R** generated by hydrogen-bonding interactions of the H_8 -BINOL-derived phosphoric acid with cyclobutanone and hydrogen peroxide. The phosphoric acid tends to donate the proton H_a to the carbonyl O_c of the cyclobuta-



Scheme 5. Proposed two-step mechanism for the phosphoric acid (**1c**) catalyzed B–V reaction.

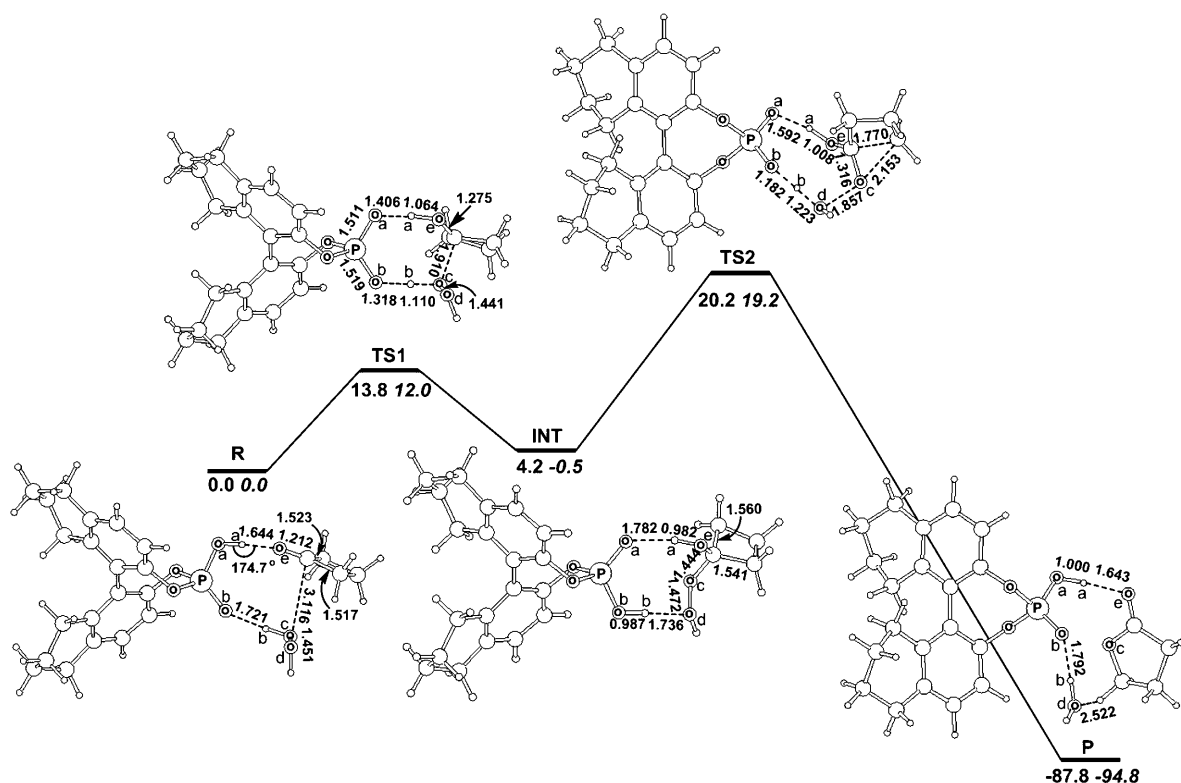


Figure 8. The optimized structures with selected bond lengths (in Å) of the reactant complex (**R**), the transition states (TS1 and TS2), the intermediate (INT) and the product (**P**). The geometries were fully optimized at the B3LYP/6-311+G** level. The relative free energies $\Delta G_{\text{B3LYP-Sol}}$ (in bold) and $\Delta G_{\text{MP2-Sol}}$ (in italic) are in kcal mol⁻¹.

none, with an O_c⋯H_a distance of 1.644 Å and a nearly linear O–H_a⋯O_e geometry (174.7°), suggesting a relatively strong intermolecular hydrogen-bonding interaction. As a result, the electrophilic character of the carbonyl carbon in **R** becomes more pronounced than that in the free cyclobutanone. Simultaneously, the phosphoryl oxygen O_b starts to accept a hydrogen (H_b) from the hydrogen peroxide, thus leading to an increase in the nucleophilicity of the oxidant. The reactants are brought in proximity in the hydrogen-bonding network, with a relative orientation that is favorable for the addition step.

The transition state for the formation of the Criegee intermediate (TS1): For the addition of hydrogen peroxide to the cyclobutanone within the hydrogen-bonding network, a moderate activation barrier in terms of Gibbs free energy was found on the potential energy surface ($\Delta G_{\text{B3LYP-Sol}} = 13.8$ kcal mol⁻¹ and $\Delta G_{\text{MP2-Sol}} = 12.0$ kcal mol⁻¹). This is reasonable considering the dual activation mode for the catalysis. TS1 retains a similar gross structure as that of **R**, but some critical changes have occurred around the phosphoric acid moiety. In TS1, the proton of the phosphoric acid (H_a) has been largely transferred to the carbonyl oxygen atom (O_c) of the cyclobutanone (H_a–O_c distance of 1.064 Å), resulting in protonation of the latter. Concurrent with this process is the incipient formation of the O_c–C bond by nucleophilic attack of hydrogen peroxide on the cyclobutanone

carbonyl group, in which the negative charge on the carbonyl oxygen is effectively trapped by protonation. As a result, the carbonyl double bond is elongated from 1.212 Å in **R** to 1.275 Å in TS1. Moreover, the proton H_b of hydrogen peroxide is transferred to the phosphoryl oxygen, rendering hydrogen peroxide more nucleophilic than in **R**. The two P–O bond lengths in TS1 are almost identical (1.511 and 1.519 Å, respectively), indicating a delocalized O–P–O bond with a bond length that is typically between the P=O double bond (ca. 1.47 Å) and the P–O single bond (ca. 1.51–1.55 Å).^[62] Thus, these data clearly indicate that the bond-forming and proton-transfer processes occur in a concerted manner through an eight-membered ring structure in TS1 as shown in Scheme 5 and Figure 8.

The phosphoric acid bound Criegee intermediate (INT): According to the B3LYP and MP2 calculations, the formation of the Criegee intermediate is expected to be reversible under the experimental conditions (with the barriers lower than 12.5 kcal mol⁻¹). In the tetrahedral peroxide moiety of INT, the peroxide–carbonyl carbon bond is fully formed, whereas the O–O bond and the two C–C bonds involving the carbonyl carbon are slightly elongated relative to those in **R**, indicating an onset weakening of these bonds. The proton transfer of the addition step has been accomplished, resulting in the regeneration of the phosphoric acid, which is engaged in hydrogen-bonding interactions with the perox-

ide moiety of INT through a nine-membered ring (Scheme 5 and Figure 8).

The transition state for the migration step (TS2): The subsequent B–V rearrangement of the INT is also a concerted step that is facilitated by the proton transfer between the Criegee intermediate and the phosphoric acid moiety. In TS2, the distal hydroperoxy oxygen O_d from the intermediate is accepting a proton H_b from the phosphoric acid to form water as a good leaving group, thus facilitating the heterolytic cleavage of the O–O bond by stabilization of the developing negative charge on O_d . Simultaneously, the methylene group that is *anti*-periplanar to O_c – O_d migrates with the incipient formation of an O–C bond (2.153 Å) and the rupture of C–C bond (1.770 Å). The migration in turn facilitates the formation of the C=O double bond, and the proton on the oxygen is ready to be transferred to the phosphoryl group of the catalyst. Animation of the imaginary frequency value of TS2 at 820.5i confirms that the rearrangement is a concerted process, with the critical bond forming and breaking being in synergy with the hydrogen migrations. The activation barrier for the rearrangement of INT is significantly higher than its formation, and thus will control the overall rate of the B–V reaction. The activation barrier of <20 kcal mol⁻¹ for this rate-determining step is compatible with the mild reaction conditions employed in the experimental studies.

The catalyst-bound γ -lactone product (P): The formation of the lactone is accomplished without loss of hydrogen bonding to the phosphoric acid, leading to the catalyst-bound γ -lactone product complex **P**. The migration is calculated to be strongly exothermic (>87 kcal mol⁻¹), indicating this step

is effectively irreversible. Thus the overall reaction is kinetically controlled, and for the asymmetric B–V reaction of 3-substituted cyclobutanones, this migration will create a chiral center in the product and will determine the enantioselectivity. The relatively strong binding of lactone to phosphoric acid has important implications for the kinetics of the reaction, and this would provide an explanation of the product inhibition as discussed above for the results of kinetic studies.

Overall, a remarkable feature of the calculated mechanism is the relay of the protons H_a and H_b , which are shuttling back and forth between the reacting species and the catalyst by hydrogen-bonding interactions, thus facilitating a concerted bond-making and -breaking process for both steps of the catalysis. This reaction pathway is consistent with the kinetic results and the mechanistic proposal by List and Müller,^[46] and it is similar to the mechanism of carboxylic acid catalyzed B–V oxidation using peracids proposed by Alvarez-Idaboy and co-workers.^[19,22,23]

Rationalization of the reactivities of different ketones towards the B–V reaction: The B–V reactions of acetone, cyclopentanone, and cyclohexanone were also examined theoretically, promoted by **1c** and using hydrogen peroxide as the oxidant. Because both the electrophilicity and hydrogen-bonding capability of these ketones can be expected to be similar to those of cyclobutanone, similar reactivity for the addition was assumed for both cyclic and acyclic ketones. Only the transition structures and the activation barriers for the rate-determining step of these reactions are calculated, and the results are shown in Figure 9. The geometries are fully optimized at the B3LYP/6-311+G** level. The barriers ($\Delta G_{\text{B3LYP-Sol}}$) for the rate-determining step of the B–V reac-

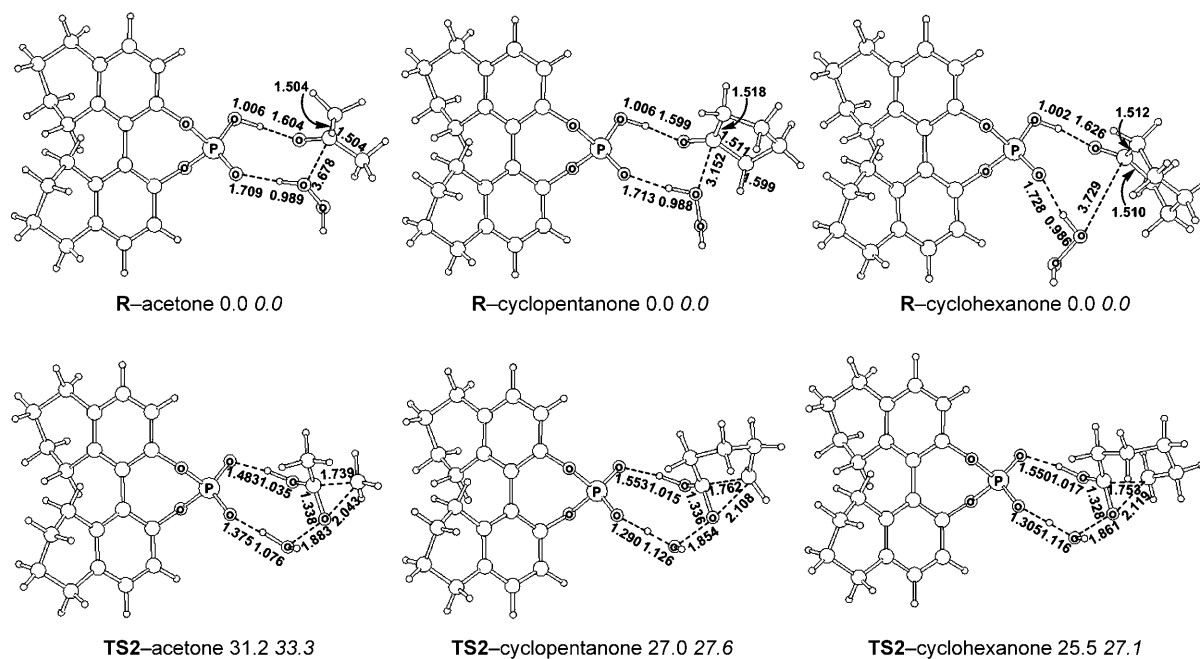


Figure 9. The calculated structures with selected bond lengths (in Å) and relative energies (in kcal mol⁻¹) ($\Delta G_{\text{B3LYP-Sol}}$ (in bold) and $\Delta G_{\text{MP2-Sol}}$ (in italic)) of the reactant complexes (**R**) and the transition states TS2 for the B–V reactions of acetone, cyclopentanone and cyclohexanone.

tions of acetone, cyclopentanone, and cyclohexanone (31.2, 27.0, and 25.5 kcal mol⁻¹, respectively) are remarkably higher than that of cyclobutanone (20.2 kcal mol⁻¹), which is consistent with their inactivity in experimental observations. This is not surprising considering the larger ring strain in cyclobutanone weakens the C–C bond and makes the migration of the methylene group relatively more facile. In the reactant complex containing cyclobutanone, the C–C bond lengths are 1.523/1.517 Å (Figure 8), whereas in acetone, cyclopentanone, and cyclohexanone, the C–C bond lengths are 1.504/1.504, 1.518/1.511, and 1.512/1.510 Å, respectively (Figure 9). Therefore, the present B–V reaction is facilitated by the large ring strain in cyclobutanone.

The origin of the enantioselectivity: The mechanistic calculation revealed that activation of both substrate and H₂O₂ by phosphoric acids constitutes the basis for these B–V reactions of cyclobutanones, and the catalyst is capable of stabilizing the TS2 of the rate-determining, stereocenter-forming, alkyl-migration step by partial proton transfer. A chiral center is created in this migration step, thus the ratio of *R* and *S* isomers in the lactone product should necessarily be dependent on the energetic differences between the competing diastereomeric transition states of this step. In the experimental investigation of the reaction, it has been found that the presence of bulky fused aryl substituents at the 3- and 3'-positions of the BINOL-derived phosphoric acid is crucial for high enantioselectivity, and variations of the stereoelectronic properties of these aryl substituents resulted in pronounced effects.^[42] On the other hand, changing the substituent at the 3-position of the cyclobutanone substrate from an aryl to an alkyl group resulted in a considerable decrease in enantioselectivity. Therefore, a (*R*)-H₈-BINOL-de-

rived phosphoric acid catalyst with bulky 3,3'-pyrenyl groups (**1b**) and 3-phenylcyclobutanone (**2a**) substrate were chosen for the calculation study, due to the high enantioselectivities obtained by using such a catalyst and also for adequate modeling of the substituent effect. Complete models of the competing transition states corresponding to the transition state of the rate-determining step (TS2) were constructed according to the designations as shown in Figure 10 and Scheme 6. To rationalize the high enantioselectivity, multi-site (three-point) interactions^[59] can be expected between the catalyst and the substrate in transition-state structures, that is, the two stabilizing hydrogen bonds as discussed above and an additional interaction between the substrate and the pyrenyl group(s) of the catalyst. It is a challenging task to predict the enantioselectivity of such large systems, in which the weak nonbonding interactions are predominant and the energy differences between transition states are expected to be very small. To achieve a better description of the weak nonbonding interactions, the PBE1PBE method^[70] was used instead of B3LYP in the enantioselectivity calculations. The 6-311+G** basis set was used for the reacting centers of the structure in Scheme 6 (central part encircled in the dashed line, but not including the bi(H₄-naphthyl) backbone atoms), whereas 6-31G* was used as the basis set for the remaining atoms. Taking the H₄-naphthyl rings in the catalyst as the reference planes, each pyrenyl group has two possible configurations, that is, *syn* or *anti* with respect to the phosphoric acid moiety. Taking the two different orientations of the phenyl group (up and down) in the cyclobutanone into consideration, for catalyst **1b** there are eight viable competing transition structures, four leading to the product with *R* configuration (*R*-*syn*-*anti*, *R*-*anti*-*syn*, *R*-*anti*-*anti*, and *R*-*syn*-*syn*) and the other four to the product with

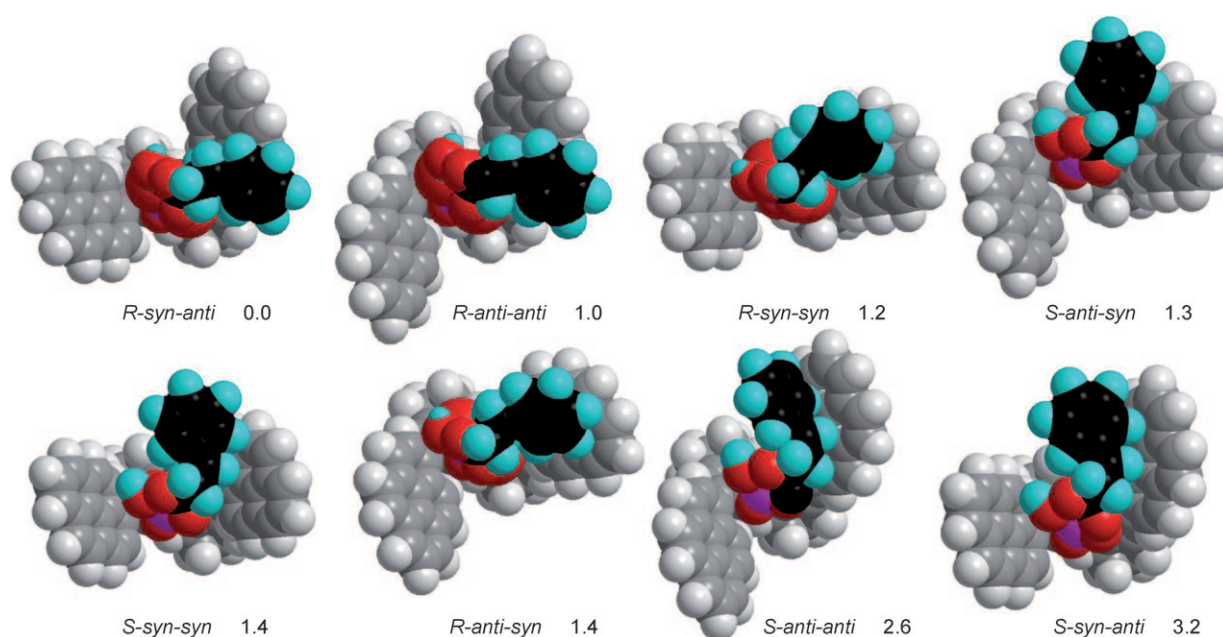
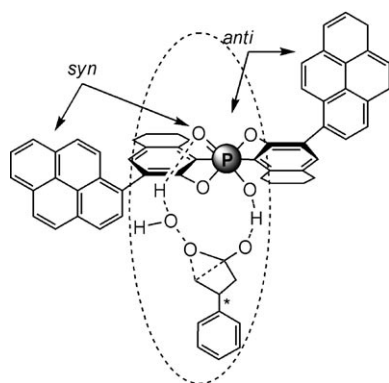


Figure 10. The eight optimized transition states with the relative free energies including solvent effect ΔG_{Total2} (in kcal mol⁻¹).



Scheme 6. The model used to calculate the enantioselectivity (6-311+G** basis set for the part of the structure encircled in the dashed line, but not including the binaphthyl backbone atoms, and the 6-31G* basis set for the remaining part).

S configuration (*S-syn-anti*, *S-anti-syn*, *S-anti-anti*, and *S-syn-syn*). These eight transition structures were fully optimized and checked by harmonic vibrational frequency calculations at the PBE1PBE/(6-311+G** and 6-31G*) level, and the solvent effect was estimated in each case by the same method as described in the previous section. The single-point energies of the eight optimized transition structures have also been calculated at the PBE1PBE/6-311+G** level. The optimized transition structures are shown in Figure 10, and the corresponding relative energies (ΔE), relative single-point energies at the PBE1PBE/6-311+G** level ($\Delta E_{(6-311+G^{**})}$), relative entropies ($\Delta S, \text{cal mol}^{-1} \text{K}^{-1}$), the contribution of ΔS to ΔG ($-T\Delta S, T=298 \text{K}$), the relative free energies in gas phase ($\Delta G_{\text{gas}}, 298 \text{K}$), the relative solvation free energy ($\Delta\Delta G_{\text{sol}}$), the total relative free energies ($\Delta G_{\text{Total}} (\Delta G_{\text{Total}} = \Delta G_{\text{gas}} + \Delta\Delta G_{\text{sol}})$), and the total relative free energies ($\Delta G_{\text{Total}2}$) corrected by $\Delta E_{(6-311+G^{**})}$ single-point energies are listed in Table 2. Gratifyingly, the calculated enantioselectivity is consistent with the experimental result. In the presence of the *R* catalyst, the most favorable transition structure is found to be *R-syn-anti*, which is $1.3 \text{ kcal mol}^{-1}$ more stable than *S-anti-syn*, the most favorable transition state among the (*S*)-producing configurations. Assuming a Boltzmann distribution of the eight transition-state struc-

tures, their energy gaps could lead to the formation of (*R*)-lactone with an *ee* value of around 73% ($\Delta G_{\text{Total}2}, 298 \text{K}$), which agrees very well with the experimental result (71% *ee* at RT).^[42]

As shown in Table 2, $\Delta E_{(6-311+G^{**})}$, $-T\Delta S$, and $\Delta\Delta G_{\text{sol}}$ are in the ranges of 1.0, 1.7, and $2.1 \text{ kcal mol}^{-1}$, respectively. Therefore, the entropy and solvent effects are decisive factors in the determination of the energy sequence of the eight transition states. For the transition structures leading to *S* products shown in Figure 10, *S-anti-anti* and *S-syn-anti* are less stable than *S-anti-syn* and *S-syn-syn*. The phenyl groups of the cyclobutanone in the first two transition states have developed very strong crowdedness with the pyrenyl group on the right side. On the contrary, in the last two cases the phenyl substituent of the cyclobutanone is staggered with the pyrenyl unit, which, being more relaxed, is accordingly more favorable in terms of entropy ($-2.143, -0.952$ vs. $-5.694, -5.054 \text{ cal mol}^{-1} \text{K}^{-1}$). Although *S-syn-anti* has a lower $\Delta E_{(6-311+G^{**})}$ value ($-0.7 \text{ kcal mol}^{-1}$), the entropy loss of this crowded structure increases the free energy by $1.5 \text{ kcal mol}^{-1}$. Here, the lower $\Delta E_{(6-311+G^{**})}$ may indicate a stable nonbonding interaction between the phenyl group of the cyclobutanone and the pyrenyl group, however, the entropy loss has larger effect on the total free energy. Similarly, the relative stabilities of the four *R*-type transition states can be easily understood. The phenyl group of the cyclobutanone overlaps with the pyrenyl group on the right side in *R-syn-syn* and *R-anti-syn* transition states, but these groups are staggered in the *R-syn-anti* and *R-anti-anti* transition states. Two factors may account for the relative stabilities of the most favorable *R-syn-anti* and *S-anti-syn* transition structures: 1) In the *S-anti-syn* transition state, the phenyl group of the cyclobutanone is to some extent congested with the pyrenyl group of the catalyst, whereas in the *R-syn-anti* transition state the phenyl group of the cyclobutanone is in some degree staggered with the pyrenyl group of the catalyst. Therefore, the *R-syn-anti* transition state is more relaxed and more favorable than the *S-anti-syn* transition state in terms of entropy (0.000 vs. $-2.143 \text{ cal mol}^{-1} \text{K}^{-1}$). 2) Compared with the *S-anti-syn* transition state, the pyrenyl group on the left in *R-syn-anti* is opened more widely, and accordingly the polar phosphoric acid is more exposed to the polar solvent, leading to favorable solvation effects (0.0 vs. $0.5 \text{ kcal mol}^{-1}$). It is notable that the ΔG_{gas} of *S-syn-syn* is $0.2 \text{ kcal mol}^{-1}$ lower than that of *R-syn-anti*. However, the relative solvation free energy of the *S-syn-syn* is $1.5 \text{ kcal mol}^{-1}$ higher than that of the *R-syn-anti*. These data clearly indicate that the solvent effect plays a significant role in the control of the enantioselectivity. Therefore, the sense of asymmetry induction will be determined not

Table 2. Various energy values for the optimized transition states.^[a]

| Transition states | $\Delta E^{[b]}$ | $\Delta E_{(6-311+G^{**})}^{[c]}$ | $\Delta S^{[d]}$ | $-T\Delta S^{[e]}$ | $\Delta G_{\text{gas}}^{[f]}$ | $\Delta\Delta G_{\text{sol}}^{[g]}$ | $\Delta G_{\text{Total}}^{[h]}$ | $\Delta G_{\text{Total}2}^{[i]}$ |
|--------------------|------------------|-----------------------------------|------------------|--------------------|-------------------------------|-------------------------------------|---------------------------------|----------------------------------|
| <i>R-syn-anti</i> | 0.0 | 0.0 | 0.000 | 0.0 | 0.0 | 0.0 | 0.0 | 0.0 |
| <i>R-anti-anti</i> | 0.0 | -0.1 | -2.767 | 0.8 | 0.7 | 0.3 | 1.0 | 0.9 |
| <i>R-syn-syn</i> | -0.6 | -1.1 | -3.720 | 1.1 | 0.7 | 1.0 | 1.7 | 1.2 |
| <i>S-anti-syn</i> | 0.1 | 0.3 | -2.143 | 0.6 | 0.6 | 0.5 | 1.1 | 1.3 |
| <i>S-syn-syn</i> | -0.6 | -0.5 | -0.952 | 0.3 | -0.2 | 1.5 | 1.3 | 1.4 |
| <i>R-anti-syn</i> | 0.5 | 0.0 | -3.278 | 1.0 | 1.4 | 0.5 | 1.9 | 1.4 |
| <i>S-anti-anti</i> | 0.1 | 0.2 | -5.694 | 1.7 | 2.0 | 0.5 | 2.5 | 2.6 |
| <i>S-syn-anti</i> | -0.9 | -0.7 | -5.054 | 1.5 | 0.9 | 2.1 | 3.0 | 3.2 |

[a] All energies are relative values in kcal mol^{-1} for the structures optimized at the PBE1PBE/(6-311+G** and 6-31G*) level. [b] The relative energy. [c] Relative single-point energy. [d] Relative entropy [$\text{cal mol}^{-1} \text{K}^{-1}$]. [e] Contribution of ΔS to ΔG (at 298 K). [f] Relative free energy in gas phase (at 298 K). [g] Relative solvation free energy. [h] Total relative free energy ($\Delta G_{\text{Total}} = \Delta G_{\text{gas}} + \Delta\Delta G_{\text{sol}}$). [i] Total relative free energies corrected by $\Delta E_{(6-311+G^{**})}$ single-point energy.

only by the entropy effect, but also critically by the solvent effect, which has been known to greatly influence the migration aptitude of the B–V reaction of some substrates.^[18,71] In fact, both the catalytic efficiency and the asymmetric induction in our phosphoric acid catalyzed B–V oxidation of **2a** using aqueous H₂O₂ were found to be strongly dependent on the nature of solvents used.^[42]

Conclusion

The mechanism of the chiral phosphoric acid catalyzed B–V reaction of cyclobutanones has been elucidated by a combined experimental and theoretical study. It was found that the involvement of a peroxyphosphate intermediate is not a viable pathway for the present reaction. The reaction follows the Michaelis–Menten kinetics typical of those encountered in enzyme-catalyzed biochemical reactions, and the resulting γ -lactone product retards the reaction by competing hydrogen bonding with the catalyst. Under the biphasic reaction conditions, the amphiphilic BINOL–phosphoric acid catalyst is saturated with hydrogen peroxide, resulting in zero order kinetics in hydrogen peroxide. The initial rate of the reaction is first order in the catalyst, but shows a more complex dependence on the concentration of the cyclobutanone substrate. These results are fully consistent with the proposed reaction sequence, in which the catalyst is actively involved in both the carbonyl addition and the subsequent rearrangement steps through hydrogen-bonding interactions with the reactants or the intermediate.

High-level quantum chemical calculations provide strong support for the two-step concerted mechanism for the catalytic reaction in which the phosphoric acid plays the role of a bifunctional catalyst to activate the reactants or the intermediate in a synergistic manner through partial proton transfer. The catalyst simultaneously increases the electrophilicity of the carbonyl carbon as a general acid and the nucleophilicity of hydrogen peroxide as a Lewis base in the addition step, and facilitates the dissociation of the poor leaving group OH from the Criegee intermediate in the rearrangement step. The overall reaction is highly exothermic, leading to the stable hydrogen-bonded lactone product. The calculated reaction profile suggests that the rearrangement of the Criegee intermediate is the rate-determining step, with an activation barrier of around 20 kcal mol⁻¹, which is compatible with the reaction conditions. The observed reactivity of the present catalytic B–V reaction is also caused in part by the ring strain in cyclobutanones. The sense of chiral induction is rationalized by the analysis of the relative energies of the competing diastereomeric transition states, in which the steric repulsion between the cyclobutanone derivative and the catalyst, as well as the entropy and solvent effects, are found to be key impact factors.

The insightful understanding of the mechanistic aspects of present catalytic asymmetric B–V oxidation may aid in the design of new catalytic systems for chiral Brønsted acid catalyzed reactions. The multiple interaction mode for the acti-

vation of reactants disclosed in the reaction, that is, the catalyst with two different binding sites in close proximity, seems to be a common feature in several mechanistic models proposed for B–V reactions, and a close resemblance in mechanism can be found between the title reaction and catalysis by carboxylic acids,^[19,22,23] metal ions,^[25] or zeolites,^[26] and thus may represent a promising approach for future catalyst development.

Experimental Section

General methods: All reactions were performed under an air atmosphere, using oven-dried glassware and magnetic stirring. Dichloromethane was distilled from powdered CaH₂ under argon prior to use. 3-Phenylcyclobutanone (**2a**),^[72] 3-*n*-hexylcyclobutanone (**2b**),^[72] and chiral phosphoric acids **1a,b**^[73] were prepared according to literature procedures. Aqueous H₂O₂ (30%) was purchased from a commercial source. NMR spectra were recorded on a Varian Mercury 300 (¹H: 300 MHz; ³¹P: 121 MHz) or Varian 400-MR (¹H: 400 MHz; ³¹P: 161 MHz) spectrometer in CDCl₃. Chemical shifts are expressed in ppm with TMS as an internal standard ($\delta = 0$ ppm) for ¹H NMR data. Coupling constants, *J*, are listed in hertz. ³¹P NMR data are reported in terms of chemical shift (δ , ppm) with 85% H₃PO₄ as the internal standard. HPLC analysis was carried out on a JASCO PU 2089 instrument with a UV 2075 detector. GC analysis was performed on an Agilent 6890N instrument with an HP-5 column. Unless stated otherwise, all solvents were purified and dried according to standard methods prior to use. Analytical GC was carried out using a HP-5 column (30 m, 0.316 mm i.d., 0.25 μ m film) and N₂ as carrier gas.

General procedures for the chiral phosphoric acid catalyzed asymmetric B–V reaction of 3-phenylcyclobutanone with different oxidants: A 5 mL Schlenk tube was charged with **1a** (7.6 mg, 10 mol%, 0.01 mmol), 3-phenylcyclobutanone **2a** (0.1 mmol), and CHCl₃ (1 mL). The mixture was stirred at room temperature and then oxidant (1.5 equiv) was added at room temperature. The reaction mixture was stirred for 12–36 h at room temperature. The reaction was quenched with an aqueous solution of Na₂SO₃ and the product **3a** was isolated by column chromatography on silica gel with petroleum ether/ethyl acetate = 6/1 as the eluent. The enantiomeric excess was determined by HPLC analysis on a Chiralcel AD-H column.

Typical procedure for the kinetic analyses: A 5 mL Schlenk tube containing a solution of **1b** (7.6 mg, 0.01 mmol), the internal standard (*n*-dodecane, 34 mg), and 3-*n*-hexylcyclobutanone (30.8 mg, 0.2 mmol) in CH₂Cl₂ (2 mL) was immersed in an oil bath and its internal temperature allowed to stabilize at 27°C. The mixture was stirred at 27°C for 5–10 min under air. An aliquot was taken at this point to establish the initial cyclobutanone/dodecane ratio, then a 30% aqueous solution of H₂O₂ (34 μ L, 1.5 equiv) was added quickly in one portion. Aliquots of 5–10 μ L were taken at the specified intervals, diluted with THF (1 mL) (note: no reaction occurs in THF!),^[42] and submitted to GC analysis. Experiments to examine the mass transfer effect with different stirring rates, product inhibition, and the initial rates of the B–V reactions were also conducted in a similar manner.

Acknowledgements

Financial support from the National Natural Science Foundation of China (no. 20872168, 20632060, 20821002), the Chinese Academy of Sciences, the Major Basic Research Development Program of China (Grant No. 2010CB833300), the Science and Technology Commission of Shanghai Municipality, and Merck Research Laboratories is gratefully acknowledged.

- [1] G. R. Krow, *Org. React.* **1993**, *43*, 251–798.
- [2] A. Baeyer, V. Villiger, *Ber. Dtsch. Chem. Ges.* **1899**, *32*, 3625–3633.
- [3] M. Renz, B. Meunier, *Eur. J. Org. Chem.* **1999**, 737–750.
- [4] a) C. Bolm in *Advances in Catalytic Processes, Vol. 2* (Ed.: M. P. Doyle), JAI Press, Greenwich, **1997**; b) G.-J. ten Brink, I. W. C. E. Arends, R. A. Sheldon, *Chem. Rev.* **2004**, *104*, 4105–4123.
- [5] G. Strukul, *Angew. Chem.* **1998**, *110*, 1256–1267; *Angew. Chem. Int. Ed.* **1998**, *37*, 1198–1209.
- [6] For a recent review, see: a) C. Jiménez-Sanchidrián, J. R. Ruiz, *Tetrahedron* **2008**, *64*, 2011–2026; for leading references in catalytic heterogeneous B–V reactions, see: b) A. Corma, L. T. Nemeth, M. Renz, S. Valencia, *Nature* **2001**, *412*, 423–425; c) A. Corma, M. T. Navarro, L. T. Nemeth, M. Renz, *Chem. Commun.* **2001**, 2190–2191; d) M. Renz, T. Blasco, A. Corma, V. Fornes, R. Jensen, L. Nemeth, *Chem. Eur. J.* **2002**, *8*, 4708–4717; e) A. Corma, M. T. Navarro, M. Renz, *J. Catal.* **2003**, *219*, 242–246.
- [7] R. Criegee, *Justus Liebigs Ann. Chem.* **1948**, *560*, 127–135.
- [8] a) K. Sato, M. Hyodo, J. Takagi, M. Aoki, R. Noyori, *Tetrahedron Lett.* **2000**, *41*, 1439–1442; b) A. Berkessel, M. R. M. Andreae, *Tetrahedron Lett.* **2001**, *42*, 2293–2295.
- [9] G.-J. ten Brink, J.-M. Vis, I. W. C. E. Arends, R. A. Sheldon, *J. Org. Chem.* **2001**, *66*, 2429–2433.
- [10] G.-J. ten Brink, J.-M. Vis, I. W. C. E. Arends, R. A. Sheldon, *Tetrahedron* **2002**, *58*, 3977–3983.
- [11] A. Berkessel, M. R. M. Andreae, H. Schmickler, J. Lex, *Angew. Chem.* **2002**, *114*, 4661–4664; *Angew. Chem. Int. Ed.* **2002**, *41*, 4481–4484.
- [12] a) H. Ichikawa, Y. Usami, M. Arimoto, *Tetrahedron Lett.* **2005**, *46*, 8665–8668; b) M. A. Goodman, M. R. Detty, *Synlett* **2006**, 1100–1104.
- [13] a) S. E. Jacobson, F. Mares, P. M. Zambri, *J. Am. Chem. Soc.* **1979**, *101*, 6938–6946; b) R. T. Taylor, L. A. Flood, *J. Org. Chem.* **1983**, *48*, 5160–5164; c) Z. B. Wang, T. Mizusaki, T. Sano, Y. Kawakami, *Bull. Chem. Soc. Jpn.* **1997**, *70*, 2567–2570; d) J. Fischer, W. F. Hölderich, *Appl. Catal. A* **1999**, *180*, 435–443.
- [14] a) C. Mazzini, J. Lebreton, R. Furstoss, *J. Org. Chem.* **1996**, *61*, 8–9; b) C. Mazzini, J. Lebreton, R. Furstoss, *Heterocycles* **1997**, *45*, 1161–1167.
- [15] S. Murahashi, S. Ono, Y. Imada, *Angew. Chem.* **2002**, *114*, 2472–2474; *Angew. Chem. Int. Ed.* **2002**, *41*, 2366–2368.
- [16] a) D. A. Singleton, M. J. Szymanski, *J. Am. Chem. Soc.* **1999**, *121*, 9455–9456; b) S. Kobayashi, H. Tanaka, H. Amii, K. Uneyama, *Tetrahedron* **2003**, *59*, 1547–1552.
- [17] L. Reyes, M. Castro, J. Cruz, M. Rubio, *J. Phys. Chem. A* **2005**, *109*, 3383–3390.
- [18] F. Grein, A. C. Chen, D. Edwards, C. M. Crudden, *J. Org. Chem.* **2006**, *71*, 861–872.
- [19] J. R. Alvarez-Idaboy, L. Reyes, N. Mora-Diez, *Org. Biomol. Chem.* **2007**, *5*, 3682–3689.
- [20] a) V. A. Stoute, M. A. Winnik, I. G. Csizmadia, *J. Am. Chem. Soc.* **1974**, *96*, 6388–6393; b) Y. Okuno, *Chem. Eur. J.* **1997**, *3*, 210–218; c) R. Cárdenas, R. Cetina, J. Lagúnez-Otero, L. Reyes, *J. Phys. Chem. A* **1997**, *101*, 192–200; d) R. Cárdenas, L. Reyes, J. Lagúnez-Otero, R. Cetina, *J. Mol. Struct.* **2000**, *516–558*, 211–225; e) H. Hanachi, N. Anoune, C. Arnaud, P. Lantéri, R. Longerey, H. Chermette, *J. Mol. Struct.* **1998**, *440–473*, 183–191; f) C. Lehtinen, V. Nevalainen, G. Brunow, *Tetrahedron* **2000**, *56*, 9375–9382.
- [21] S. Yamabe, S. Yamazaki, *J. Org. Chem.* **2007**, *72*, 3031–3041.
- [22] J. R. Alvarez-Idaboy, L. Reyes, J. Cruz, *Org. Lett.* **2006**, *8*, 1763–1765.
- [23] J. R. Alvarez-Idaboy, L. Reyes, *J. Org. Chem.* **2007**, *72*, 6580–6583.
- [24] P. Carlqvist, R. Eklund, T. Brinck, *J. Org. Chem.* **2001**, *66*, 1193–1199.
- [25] a) R. R. Sever, T. W. Root, *J. Phys. Chem. B* **2003**, *107*, 10521–10530; b) R. R. Sever, T. W. Root, *J. Phys. Chem. B* **2003**, *107*, 10848–10862.
- [26] a) M. Boronat, A. Corma, M. Renz, G. Sastre, P. M. Viruela, *Chem. Eur. J.* **2005**, *11*, 6905–6915; b) A. Corma, L. T. Nemeth, M. Renz, S. Valencia, *Nature* **2001**, *412*, 423–425; c) A. Corma, M. T. Navarro, L. T. Nemeth, M. Renz, *Chem. Commun.* **2001**, 2190–2191; d) M. Renz, T. Blasco, A. Corma, V. Fornés, R. Jensen, L. Nemeth, *Chem. Eur. J.* **2002**, *8*, 4708–4717; e) A. Corma, M. T. Navarro, M. Renz, *J. Catal.* **2003**, *219*, 242–246.
- [27] Q. P. Long, H. B. Ji, S. S. Lu, *J. Mol. Struct.* **2009**, *917–938*, 117–127.
- [28] M. D. Mihovilovic, F. Rudroff, B. Grotzl, *Curr. Org. Chem.* **2004**, *8*, 1057–1069.
- [29] S. M. Roberts, P. W. H. Wan, *J. Mol. Catal. B* **1998**, *4*, 111–136.
- [30] M. D. Mihovilovic, *Curr. Org. Chem.* **2006**, *10*, 1265–1287.
- [31] a) C. Bolm, G. Schlingloff, K. Weickhardt, *Angew. Chem.* **1994**, *106*, 1944–1946; *Angew. Chem. Int. Ed. Engl.* **1994**, *33*, 1848–1849; b) A. Gusso, C. Baccin, F. Pinna, G. Strukul, *Organometallics* **1994**, *13*, 3442–3451.
- [32] a) C. Bolm, G. Schlingloff, *J. Chem. Soc. Chem. Commun.* **1995**, 1247–1248; b) C. Bolm, T. K. K. Luong, G. Schlingloff, *Synlett* **1997**, 1151–1152; c) Y. G. Peng, X. M. Feng, K. B. Yu, Z. Li, Y. Z. Jiang, C. H. Yeung, *J. Organomet. Chem.* **2001**, *619*, 204–208.
- [33] a) C. Paneghetti, R. Cavagnin, F. Pinna, G. Strukul, *Organometallics* **1999**, *18*, 5057–5065; b) M. Colladon, A. Scarso, G. Strukul, *Synlett* **2006**, 3515–3520.
- [34] M. Lopp, A. Paju, T. Kanger, T. Pehk, *Tetrahedron Lett.* **1996**, *37*, 7583–7586.
- [35] T. Uchida, T. Katsuki, *Tetrahedron Lett.* **2001**, *42*, 6911–6914.
- [36] a) A. Watanabe, T. Uchida, K. Ito, T. Katsuki, *Tetrahedron Lett.* **2002**, *43*, 4481–4485; b) A. Watanabe, T. Uchida, Y. Irie, T. Katsuki, *Proc. Natl. Acad. Sci. USA* **2004**, *101*, 5737–5742.
- [37] C. Bolm, O. Beckmann, A. Cosp, C. Palazzi, *Synlett* **2001**, 1461–1463.
- [38] a) C. Bolm, O. Beckmann, T. Kuhn, C. Palazzi, W. Adam, P. B. Rao, C. R. Saha-Möllner, *Tetrahedron: Asymmetry* **2001**, *12*, 2441–2446; b) C. Bolm, J.-C. Frison, Y. Zhang, W. D. Wulff, *Synlett* **2004**, 1619–1621; c) J.-C. Frison, C. Palazzi, C. Bolm, *Tetrahedron* **2006**, *62*, 6700–6706.
- [39] A. V. Malkov, F. Friscourt, M. Bell, M. E. Swarbrick, P. Kočovský, *J. Org. Chem.* **2008**, *73*, 3996–4003.
- [40] Y. Miyake, Y. Nishibayashi, S. Uemura, *Bull. Chem. Soc. Jpn.* **2002**, *75*, 2233–2237.
- [41] G. Peris, S. J. Miller, *Org. Lett.* **2008**, *10*, 3049–3052.
- [42] S. Xu, Z. Wang, X. Zhang, X. Zhang, K. Ding, *Angew. Chem.* **2008**, *120*, 2882–2885; *Angew. Chem. Int. Ed.* **2008**, *47*, 2840–2843.
- [43] a) M. D. Del Todesco Frisone, F. Pinna, G. Strukul, *Organometallics* **1993**, *12*, 148–156; b) R. Gavagnin, M. Cataldo, F. Pinna, G. Strukul, *Organometallics* **1998**, *17*, 661–667.
- [44] A. Brunetta, P. Sgarbossa, G. Strukul, *Catal. Today* **2005**, *99*, 227–232.
- [45] a) C. Girard, H. B. Kagan, *Angew. Chem.* **1998**, *110*, 3088–3127; *Angew. Chem. Int. Ed.* **1998**, *37*, 2922–2959; b) T. Satyanarayana, S. Abraham, H. B. Kagan, *Angew. Chem.* **2009**, *121*, 464–503; *Angew. Chem. Int. Ed.* **2009**, *48*, 456–494.
- [46] B. List, S. Müller, *Synfacts* **2008**, 640.
- [47] Y. Ogata, K. Tomizawa, T. Ikeda, *J. Org. Chem.* **1978**, *43*, 2417–2419.
- [48] D. Uraguchi, M. Terada, *J. Am. Chem. Soc.* **2004**, *126*, 5356–5357.
- [49] D. Uraguchi, K. Sorimachi, M. Terada, *J. Am. Chem. Soc.* **2005**, *127*, 9360–9361.
- [50] a) S. J. Connon, *Angew. Chem.* **2006**, *118*, 4013–4016; *Angew. Chem. Int. Ed.* **2006**, *45*, 3909–3912; b) T. Akiyama, J. Itoh, K. Fuchibe, *Adv. Synth. Catal.* **2006**, *348*, 999–1010.
- [51] a) T. Akiyama, *Chem. Rev.* **2007**, *107*, 5744–5758; b) M. Terada, *Chem. Commun.* **2008**, 4097–4112; c) L.-Z. Gong, X.-H. Chen, X.-Y. Xu, *Chem. Eur. J.* **2007**, *13*, 8920–8926; d) A. G. Doyle, E. N. Jacobsen, *Chem. Rev.* **2007**, *107*, 5713–5743.
- [52] After many trials we were unable to synthesize the peroxy derivative of the BINOL phosphoric acid or its *tert*-butyl peroxyphosphate analogue. Nevertheless, the analogue diethyl *tert*-butyl phosphate and diethyl *tert*-butyl peroxyphosphate can be easily synthesized according to literature procedures: a) N. Yoshihiro, A. Yasushi, *Chem. Pharm. Bull.* **1986**, *34*, 3121–3129; b) G. Sosnovsky, E. H. Zaret, *J.*

- Org. Chem.* **1969**, *34*, 968–970. ³¹P NMR spectra indicate a down-field change in chemical shift upon peroxyphosphate formation, see Figure S1 in the Supporting Information.
- [53] a) D. G. Blackmond, *Angew. Chem.* **2005**, *117*, 4374–4393; *Angew. Chem. Int. Ed.* **2005**, *44*, 4302–4320; b) J. S. Mathew, M. Klussmann, H. Iwamura, F. Valera, A. Futran, E. A. C. Emanuelsson, D. G. Blackmond, *J. Org. Chem.* **2006**, *71*, 4711–4722.
- [54] A. Zanardo, F. Pinna, R. A. Michelin, G. Strukul, *Inorg. Chem.* **1988**, *27*, 1966–1973.
- [55] M. Colladon, A. Scarso, P. Sgarbossa, R. A. Michelin, G. Strukul, *J. Am. Chem. Soc.* **2007**, *129*, 7680–7689.
- [56] T. Dorn, A.-C. Chamayou, C. Janiak, *New J. Chem.* **2006**, *30*, 156–167.
- [57] H. Lineweaver, D. Burk, *J. Am. Chem. Soc.* **1934**, *56*, 658–666.
- [58] For examples: a) T. Akiyama, H. Morita, J. Itoh, K. Fuchibe, *Org. Lett.* **2005**, *7*, 2583–2585; b) M. Terada, K. Machioka, K. Sorimachi, *Angew. Chem.* **2006**, *118*, 2312–2315; *Angew. Chem. Int. Ed.* **2006**, *45*, 2254–2257; c) Y.-X. Jia, J. Zhong, S.-F. Zhu, C.-M. Zhang, Q.-L. Zhou, *Angew. Chem.* **2007**, *119*, 5661–5663; *Angew. Chem. Int. Ed.* **2007**, *46*, 5565–5567; d) Q.-X. Guo, H. Liu, C. Guo, S.-W. Luo, Y. Gu, L.-Z. Gong, *J. Am. Chem. Soc.* **2007**, *129*, 3790–3791; e) M. Rueping, W. Leawsuwan, A. P. Antonchick, B. J. Nachtsheim, *Angew. Chem.* **2007**, *119*, 2143–2146; *Angew. Chem. Int. Ed.* **2007**, *46*, 2097–2100; f) Q. Kang, Z.-A. Zhao, S.-L. You, *J. Am. Chem. Soc.* **2007**, *129*, 1484–1485; g) Q. Kang, X.-J. Zhen, S.-L. You, *Chem. Eur. J.* **2008**, *14*, 3539–3542; h) X. Wang, B. List, *Angew. Chem.* **2008**, *120*, 1135–1138; *Angew. Chem. Int. Ed.* **2008**, *47*, 1119–1122.
- [59] L. Simon, J. M. Goodman, *J. Am. Chem. Soc.* **2008**, *130*, 8741–8747.
- [60] T. Marcelli, P. Hammar, F. Himo, *Chem. Eur. J.* **2008**, *14*, 8562–8571.
- [61] L. Simon, J. M. Goodman, *J. Am. Chem. Soc.* **2009**, *131*, 4070–4077.
- [62] M. Yamanaka, T. Hirata, *J. Org. Chem.* **2009**, *74*, 3266–3271.
- [63] F. Q. Shi, B. A. Song, *Org. Biomol. Chem.* **2009**, *7*, 1292–1298.
- [64] a) P. Hohenberg, W. Kohn, *Phys. Rev. B* **1964**, *136*, B864–B871; b) W. Kohn, L. J. Sham, *Phys. Rev.* **1965**, *140*, A1133–A1138.
- [65] a) M. Head-Gordon, J. A. Pople, M. J. Frisch, *Chem. Phys. Lett.* **1988**, *153*, 503–506; b) M. J. Frisch, M. Head-Gordon, J. A. Pople, *Chem. Phys. Lett.* **1990**, *166*, 275–280; c) M. J. Frisch, M. Head-Gordon, J. A. Pople, *Chem. Phys. Lett.* **1990**, *166*, 281–289.
- [66] Gaussian 03, Revision D.01, M. J. Frisch, G. W. Trucks, H. B. Schlegel, G. E. Scuseria, M. A. Robb, J. R. Cheeseman, J. A. Montgomery, Jr., T. Vreven, K. N. Kudin, J. C. Burant, J. M. Millam, S. S. Iyengar, J. Tomasi, V. Barone, B. Mennucci, M. Cossi, G. Scalmani, N. Rega, G. A. Petersson, H. Nakatsuji, M. Hada, M. Ehara, K. Toyota, R. Fukuda, J. Hasegawa, M. Ishida, T. Nakajima, Y. Honda, O. Kitao, H. Nakai, M. Klene, X. Li, J. E. Knox, H. P. Hratchian, J. B. Cross, V. Bakken, C. Adamo, J. Jaramillo, R. Gomperts, R. E. Stratmann, O. Yazyev, A. J. Austin, R. Cammi, C. Pomelli, J. W. Ochterski, P. Y. Ayala, K. Morokuma, G. A. Voth, P. Salvador, J. J. Dannenberg, V. G. Zakrzewski, S. Dapprich, A. D. Daniels, M. C. Strain, O. Farkas, D. K. Malick, A. D. Rabuck, K. Raghavachari, J. B. Foresman, J. V. Ortiz, Q. Cui, A. G. Baboul, S. Clifford, J. Cioslowski, B. B. Stefanov, G. Liu, A. Liashenko, P. Piskorz, I. Komaromi, R. L. Martin, D. J. Fox, T. Keith, M. A. Al-Laham, C. Y. Peng, A. Nanayakkara, M. Challacombe, P. M. W. Gill, B. Johnson, W. Chen, M. W. Wong, C. Gonzalez, J. A. Pople, Gaussian, Inc., Wallingford CT, **2004**.
- [67] K. M. Waltz, P. J. Carroll, P. J. Walsh, *Organometallics* **2004**, *23*, 127–134.
- [68] a) A. D. Becke, *J. Chem. Phys.* **1993**, *98*, 5648–5652; b) C. T. Lee, W. T. Yang, R. G. Parr, *Phys. Rev. B* **1988**, *37*, 785–789.
- [69] a) E. Cancès, B. Mennucci, J. Tomasi, *J. Chem. Phys.* **1997**, *107*, 3032–3041; b) M. Cossi, V. Barone, B. Mennucci, J. Tomasi, *Chem. Phys. Lett.* **1998**, *286*, 253–260.
- [70] a) J. P. Perdew, K. Burke, M. Ernzerhof, *Phys. Rev. Lett.* **1996**, *77*, 3865–3868; b) J. P. Perdew, K. Burke, M. Ernzerhof, *Phys. Rev. Lett.* **1997**, *78*, 1396–1396.
- [71] C. Lehtinen, V. Nevalainen, G. Brunow, *Tetrahedron* **2001**, *57*, 4741–4751.
- [72] L. R. Krepski, A. Hassner, *J. Org. Chem.* **1978**, *43*, 2879–2882.
- [73] For the synthesis of racemic BINOL, see: a) K. Ding, Y. Wang, L. Zhang, Y. Wu, T. Matsuura, *Tetrahedron* **1996**, *52*, 1005–1010; for the resolution of BINOL, see: b) Y. Wang, J. Sun, K. Ding, *Tetrahedron* **2000**, *56*, 4447–4451; c) H. Du, Y. Wang, J. Sun, J. Meng, K. Ding, *Tetrahedron Lett.* **2002**, *43*, 5273–5276; for the synthesis of H₈-BINOL, see: d) H. Guo, K. Ding, *Tetrahedron Lett.* **2000**, *41*, 10061–10064; for the synthesis of BINOL and H₈-BINOL derivatives, see: e) J. Long, J. Hu, X. Shen, B. Ji, K. Ding, *J. Am. Chem. Soc.* **2002**, *124*, 10–11; for the synthesis of chiral phosphoric acids, see: f) J. Inanaga (Tosoh Corporation, Japan), EP1134209, **2001**.

Received: September 30, 2009
Published online: January 27, 2010